Boundary Element Method Solution in the Time Domain For a Moving Time-Dependent Force

Nielsen, Søren R.K.; Kirkegaard, Poul Henning; Rasmussen, K. M.

Published in:
Computers & Structures

DOI (link to publication from Publisher):
10.1016/S0045-7949(00)00175-9

Publication date:
2001

Document Version
Publisher's PDF, also known as Version of record

PERGAMON

Computers and Structures 79 (2001) 691–701

Computers & Structures

www.elsevier.com/locate/compstruc

Boundary element method solution in the time domain for a moving time-dependent force

K.M. Rasmussen, S.R.K. Nielsen *, P.H. Kirkegaard

Department of Building Technology and Structural Engineering, Aalborg University, Sohngaardsholmsvej 57, DK-9000 Aalborg, Denmark

Received 24 August 1999; accepted 16 July 2000

Abstract

The problem of a moving time dependent concentrated force on the surface of an elastic halfspace is of interest in the analysis of traffic generated noise. The Boundary element method (BEM) is superior to the Finite element method (FEM) in solving such problems due to its inherent ability so satisfy the radiation conditions exactly. In this paper a model based on the BEM is formulated for the solution of the mentioned problem. A numerical solution is obtained for the 2D plane strain case, and comparison is made with the results obtained from a corresponding FEM solution with an impedance absorbing boundary condition. © 2001 Published by Elsevier Science Ltd. All rights reserved.

Keywords: Boundary element method; Moving force; Wave propagation; Stress-waves; Soil dynamics

1. Introduction

Traffic induced vibrations are known sources of discomfort and damage problems in nearby buildings, either directly in the form of vibrations of the buildings or through structure borne acoustic noise. During the last couple of decades highway induced noise has become an increasing problem due to the increase of the general amount of traffic. Besides the average weight and velocity of trucks have increased significantly, which further has emphasized the problems of traffic induced vibrations. Also train induced vibrations have been given some attention in recent years, mainly due to the dramatic increase in speed, see e.g. Ref. [6]. Okumura et al. [11] showed through extensive measurements how noise and vibrations from trains depend on distance from tracs, railway structure, train length and speed of the train. Trochides [17] developed a numerical method giving rough estimates of the vibrations from subway trains. Krylov [8] used a relatively simple numerical method to calculate the Rayleigh surface ground vibrations from superfast trains. The method shows that a very large increase in vibration level may occur if the train speed exceeds the velocity of Rayleigh surface waves.

The increased speed and the still greater number of underground railway systems in urban areas have resulted in still larger vibration problems. An considerable effort has been made to minimize or soften the effects of the traffic induced vibrations. Chouw et al. [4] investigated how to reduce train induced vibrations by using different railway constructions and the influence of soft soils. Nelson [10] discussed different railway constructions used in the US to reduce train induced vibrations.

With respect to analysis, semi-empirical methods for estimating the vibrations have been introduced by Madshus et al. [9], who introduced a semi-empirical method for predicting low frequency vibration in areas with soft ground conditions. The method is based on a statistical formulation and a large number of vibrations measurements. Several numerical methods used to estimate the vibrations have been introduced, but mainly in the frequency domain.

* Corresponding author. Tel.: +45-9635-8573; fax: +45-9814-8243.

E-mail address: soren.nielsen@civil.auc.dk (S.R.K. Nielsen).

0045-7949/01/$ - see front matter
PII: S0045-7949(00)00175-9

In the papers by Suiker et al. [15,16] wave propagation in a stratified halfspace consisting of an elastic granular upper layer and a lower half infinite elastic continuum was investigated. An analytical solution using a second-gradient continuum formulation and a Cosserat continuum formulation was used to study the critical behaviour of the stratisfied medium under a moving vibrating load. Suiker et al. used a relatively complex analytical method in their study whereas the present study presents a relatively simple correction of the well known time domain BEM giving a solution to moving load problems.

Pan and Atluri [12] presented a coupled Boundary element method/Finite element method (BEM/FEM) approach to the problem of a moving load on a finite elastic plate, resting on an elastic halfspace. The time domain BEM was solved using analytical time integration as for the present study. However Pan ans Atluri used standard BEM and FEM formulations to study moving loads whereas the present study introduces a new moving BEM formulation.

Regarding analysis of ground surface motions numerous papers have been published, but especially regarding vibration isolation by trenches, soil layers or piles the work by Beskos and Vardoulakis [2] should be mentioned. For a complete overview of the latest developments within BEM the comprehensive review of BEM for the solution of elastodynamic problems covering the period 1986–1996 should be consulted [3].

Simulation of traffic induced vibrations in an elastic medium can be achieved as a sum of moving concentrated time-varying forces due to the superposition principle. Thus, the generic problem that must be solved to simulate traffic induced vibrations is the problem of a moving time dependent force on the surface of an elastic halfspace. When using the BEM or FEM to solve this problem an important problem arises. With an element mesh of finite size the moving force will soon move beyond the boundary of the mesh. Therefore, it will be preferable to formulate the problem in a coordinate system moving along with the force, i.e. a convective formulation should be used.

FEM formulations in convected coordinates where the mesh is following the force are well known. If this is coupled with transmitting boundaries an efficient method for modelling transient problems of moving forces on infinite media arises, see e.g. Ref. [7].

In this paper Green's functions in the time domain for the displacements and surface tractions are formulated in a coordinate system moving along with the force. Thereby a BEM formulation in a moving coordinate system is established similar to the method of coupling convected coordinates with absorbing boundaries for the FEM. Numerical results obtained by the BEM have been indicated for a 2D plane strain problem, and the results are compared to those obtained by the FEM.

2. Formulation of boundary element equations for a moving force

Let $U_{ik}(\mathbf{x},t;\xi)$ signify the displacement field in the coordinate direction i from a concentrated time dependent force $f(t)$ applied at position ξ in direction k in a homogeneous, isotropic and linear elastic medium with the Lamé constants λ and μ and the mass density ρ. Assuming the media at rest at the time $t=0$ the displacement is given as

$$U_{ik}(\mathbf{x},t;\xi)=\int_0^t g_{ik}(\mathbf{x},t;\xi,\tau)f(\tau)\,\mathrm{d}\tau. \tag{1}$$

Green's function for the displacement field $g_{ik}(\mathbf{x},t;\xi,\tau)$ is the solution to the differential equations

$$\frac{\partial\sigma_{ijk}}{\partial x_j}-\rho\frac{\partial^2 g_{ik}}{\partial t^2}+\delta_{ik}\delta(\mathbf{x}-\xi)\delta(t-\tau)=0. \tag{2}$$

$\sigma_{ijk}(\mathbf{x},t;\xi,\tau)$ is the stress tensor derived from the displacement field $g_{ik}(\mathbf{x},t;\xi,\tau)$, δ_{ik}, the Kronecker's delta and $\delta(t)$, the Dirac's delta function. Further, the summation convention for Cartesian tensors has been used. Next, consider a concentrated force moving at a constant velocity v_i in a linear elastic media, see Fig. 1.

Next, a $(\tilde{x}_1,\tilde{x}_2,\tilde{x}_3)$-coordinate system is introduced, which follows the moving force. $\tilde{\xi}_i$ signifies the coordinates of the force, and $\tilde{g}_{ik}(\tilde{\mathbf{x}},t;\tilde{\xi},\tau)$ is the Green's function for the displacement $\tilde{u}_i(\tilde{\mathbf{x}},t)$ in the moving coordinate system. The two coordinate systems coalesce at the time $t=\tau$ which corresponds to the Galilean transformation

$$x_i=\tilde{x}_i+v_i(t-\tau). \tag{3}$$

The equations of motion in the moving coordinate system are expressed by introducing the partial differentiation operators

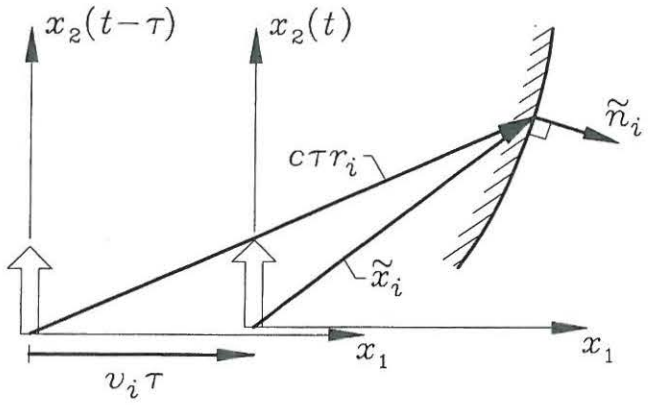

Fig. 1. Moving force in fixed and moving coordinate systems.

$$\begin{aligned}
\frac{\partial}{\partial x_j} &= \frac{\partial}{\partial \tilde{x}_j}, \\
\left.\frac{\partial}{\partial t}\right|_{x_j} &= \left.\frac{\partial}{\partial t}\right|_{\tilde{x}_j} - v_j \frac{\partial}{\partial \tilde{x}_j}, \\
\left.\frac{\partial^2}{\partial t^2}\right|_{x_j} &= \left.\frac{\partial^2}{\partial t^2}\right|_{\tilde{x}_j} - 2v_j \left.\frac{\partial^2}{\partial \tilde{x}_j \partial t}\right|_{\tilde{x}_j} + v_j v_k \frac{\partial^2}{\partial \tilde{x}_j \partial \tilde{x}_k}.
\end{aligned} \tag{4}$$

Hereby the partial differential equations for the Green's functions in the moving coordinate system read

$$\begin{aligned}
&\frac{\partial \tilde{\sigma}_{ijk}}{\partial \tilde{x}_j} - \rho\left(\frac{\partial^2 \tilde{g}_{ik}}{\partial t^2} - 2v_j \frac{\partial^2 \tilde{g}_{ik}}{\partial \tilde{x}_j \partial t} + v_j v_l \frac{\partial^2 \tilde{g}_{ik}}{\partial \tilde{x}_j \partial \tilde{x}_l}\right) \\
&\quad + \delta_{ik}\delta(\tilde{\mathbf{x}} - \tilde{\boldsymbol{\xi}})\delta(t-\tau) = 0.
\end{aligned} \tag{5}$$

Introducing the coordinate transformation (3) into Eq. (5) the following equations for $\tilde{g}_{ij}$ is found as a function of the fixed coordinates x_i:

$$\frac{\partial \tilde{\sigma}_{ijk}}{\partial x_j} - \rho \frac{\partial^2 \tilde{g}_{ik}}{\partial t^2} + \delta_{ik}\delta(\mathbf{x} - \mathbf{v}(t-\tau) - \tilde{\boldsymbol{\xi}})\delta(t-\tau) = 0. \tag{6}$$

Since $\delta(\mathbf{x} - \mathbf{v}(t-\tau) - \tilde{\boldsymbol{\xi}})\delta(t-\tau) = \delta(\mathbf{x} - \tilde{\boldsymbol{\xi}})\delta(t-\tau)$, the solution of Eq. (6) becomes $g_{ik}(\mathbf{x}, t; \tilde{\boldsymbol{\xi}}, \tau)$. The solution to Eq. (5) can then be expressed in terms of the Green's function for the displacement field in the fixed coordinate system in the following way:

$$\begin{aligned}
\tilde{g}_{ik}(\tilde{\mathbf{x}}, t; \tilde{\boldsymbol{\xi}}, \tau) &= g_{ik}(\mathbf{x}, t-\tau; \tilde{\boldsymbol{\xi}}, 0) \\
&= g_{ik}(\tilde{\mathbf{x}} + \mathbf{v}(t-\tau), t-\tau; \tilde{\boldsymbol{\xi}}, 0).
\end{aligned} \tag{7}$$

The Green's function for Cauchy's stress tensor $\tilde{\sigma}_{ijk} \times (\tilde{\mathbf{x}}, t; \tilde{\boldsymbol{\xi}}, \tau)$ is obtained upon insertion of the solution of Eq. (7) into the constitutive equations for the considered linear elastic material. Since these only involve spatial differential operations with respect to $\mathbf{x}$, the result is seen to be

$$\tilde{\sigma}_{ijk}(\tilde{\mathbf{x}}, t; \tilde{\boldsymbol{\xi}}, \tau) = \sigma_{ijk}(\tilde{\mathbf{x}} + \mathbf{v}(t-\tau), t-\tau; \tilde{\boldsymbol{\xi}}, 0). \tag{8}$$

Hence, a BEM formulation in the moving coordinate system that calculates the displacement field following the force can be established by using the formal Green's functions $\tilde{g}_{ik}(\tilde{\mathbf{x}}, t; \tilde{\boldsymbol{\xi}}, \tau)$ and $\tilde{\sigma}_{ijk}(\tilde{\mathbf{x}}, t; \tilde{\boldsymbol{\xi}}, \tau)$, as given by Eqs. (7) and (8), instead of the original ones. Notice that this result is generally valid for linear materials whether these are homogeneous and isotropic or not.

3. Boundary element formulation

Green's function for the displacement field in linear elastic homogeneous and isotropic fields, $g_{ik}(\mathbf{x}, t; \xi, 0)$ is well known and can be found in e.g. Ref. [5]. For 2D and 3D elastic problems these read

$$\begin{aligned}
g_{ik}(\mathbf{x}, t; \xi, 0) = {} & \frac{H(c_P t - r)}{2\pi\rho c_P}\left(\frac{r_i r_k}{r^4}\frac{2c_P^2 t^2 - r^2}{\sqrt{c_P^2 t^2 - r^2}} - \frac{\delta_{ik}}{r^2}\sqrt{c_P^2 t^2 - r^2}\right) \\
& - \frac{H(c_S t - r)}{2\pi\rho c_S}\left(\frac{r_i r_k}{r^4}\frac{2c_S^2 t^2 - r^2}{\sqrt{c_S^2 t^2 - r^2}} - \frac{\delta_{ik}}{r^2}\sqrt{c_S^2 t^2 - r^2} - \frac{\delta_{ik}}{\sqrt{c_S^2 t^2 - r^2}}\right),
\end{aligned} \tag{9}$$

$$\begin{aligned}
g_{ik}(\mathbf{x}, t; \xi, 0) = {} & \frac{1}{4\pi\rho}\left(3\frac{r_i r_k}{r^5} - \frac{\delta_{ik}}{r^3}\right) t\left(H\left(t - \frac{r}{c_P}\right) - H\left(t - \frac{r}{c_S}\right)\right) + \frac{1}{4\pi\rho c_P^2}\frac{r_i r_k}{r^3}\delta\left(t - \frac{r}{c_P}\right) \\
& + \frac{1}{4\pi\rho c_S^2}\left(\frac{\delta_{ik}}{r} - \frac{r_i r_k}{r^3}\right)\delta\left(t - \frac{r}{c_S}\right),
\end{aligned} \tag{10}$$

where $r = |\mathbf{x} - \xi|$, and $c_P = \sqrt{(\lambda + 2\mu)/\rho}$ and $c_S = \sqrt{\mu/\rho}$ denotes the phase velocities of P- and S-waves. In the 2D case the free indices i, j, k are running over the range 1, 2. λ and μ for the plane strain case are the same as for the 3D case. However, well known modifications of these constants are needed in the plane stress case. $H(\cdot)$ is the Heaviside unit step function defined as

$$H(x) = \begin{cases} 1, & x \geqslant 0, \\ 0, & x < 0. \end{cases} \tag{11}$$

Next, the Green's function for the surface traction may derived from $t_{ik}(\mathbf{x}, t; \xi, 0) = \sigma_{ijk}(\mathbf{x}, t; \xi, 0)n_j(\mathbf{x})$, $\sigma_{ijk}(\mathbf{x}, t; \xi, 0) = \delta_{ij}\lambda\partial/\partial x_l g_{lk}(\mathbf{x}, t; \xi, 0) + \mu(\partial/\partial x_j g_{ik}(\mathbf{x}, t; \xi, 0) + \partial/\partial x_i g_{jk}(\mathbf{x}, t; \xi, 0))$. The explicit expression of the Green's function (7) follows from Eqs. (9) and (10) upon replacing t with $t - \tau$, $\mathbf{x}$ with $\tilde{\mathbf{x}} + \mathbf{v}(t-\tau)$ and ξ with $\tilde{\xi}$. Formally the Green functions are obtained upon using $r = |\tilde{\mathbf{x}} + \mathbf{v}(t-\tau) - \tilde{\xi}|$ in Eqs. (9) and (10).

Using Betti's reciprocal theorem and the symmetry properties of Green's function, Somigliani's identity is obtained

$$\begin{aligned}
C(\tilde{\mathbf{x}})u_i(\tilde{\mathbf{x}}, t) = {} & \int_S \int_0^t g_{ik}(\tilde{\mathbf{x}}, t-\tau; \tilde{\boldsymbol{\xi}}, 0)t_k(\xi, \tau; \mathbf{n}(\tilde{\boldsymbol{\xi}}))\,\mathrm{d}\tau\,\mathrm{d}S_{(\tilde{\xi})} \\
& - \int_S \int_0^t \sigma_{ijk}(\mathbf{x}, t-\tau; \tilde{\boldsymbol{\xi}}, 0)n_j(\tilde{\mathbf{x}})u_k(\tilde{\boldsymbol{\xi}}, \tau)\,\mathrm{d}\tau\,\mathrm{d}S_{(\tilde{\xi})}.
\end{aligned} \tag{12}$$

$C(\tilde{\mathbf{x}})$ is a parameter which is 1 for $\tilde{\mathbf{x}}$ in the interior, 0 for $\tilde{\mathbf{x}}$ in the exterior and 1/2 for $\tilde{\mathbf{x}}$ on the surface of the domain if the surface is smooth. For surface points with sharp corners special attention is needed. Discretization of Somigliana's identity in 3D yields

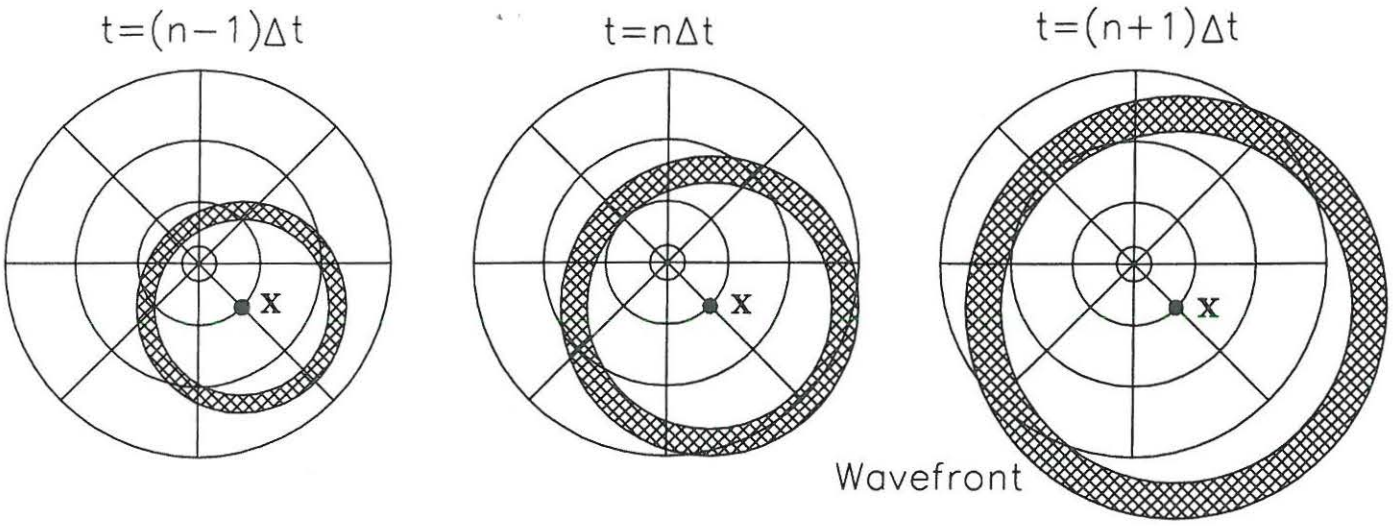

Fig. 2. A wave front emerging from the source point.

$$C(\tilde{\mathbf{x}})u_i^+(\tilde{\mathbf{x}},t) = \sum_{m=1}^{M}\sum_{n=1}^{N}\int_{S^m} g_{ik}(\mathbf{x},t;\tilde{\xi}(\tilde{\eta}),0) * N^{(m,n)}(\tilde{\eta})\cdot t_k^{(m,n)}(t)\det(\mathbf{J}^{(m)}(\tilde{\eta}))\,\mathrm{d}S_{(\tilde{\eta})} - \sum_{m=1}^{M}\sum_{n=1}^{N}\int_{S^m} t_{ik}(\tilde{\mathbf{x}},t;\tilde{\xi}(\tilde{\eta}),0) * N^{(m,n)}(\tilde{\eta})u_k^{(m,n)}(t)\det(\mathbf{J}^{(m)}(\tilde{\eta}))\,\mathrm{d}S_{(\tilde{\eta})}, \quad (13)$$

where M is the number of elements into which the surface has been divided, N, the number of nodal points within each element, $*$, an operator indicating the convolution integral over time, η, the local axis over which the integration is performed, $N^{(m,n)}(\tilde{\eta})$, $\det(\mathbf{J}^{(m)}(\tilde{\eta}))$, $t_k^{(m,n)}(t)$ and $u_k^{(m,n)}(t)$ are the shape functions, the Jacobian and the nodal values of the displacement field belonging to element m. The convolution integral in Eq. (13) is solved analytically, see Section 4.

The discontinuity of the Green's functions causes numerical troubles, when the integration in Eq. (13) over the surface S_m is performed with ordinary numerical element by element integration. In order to enhance the accuracy of the numerical integration scheme a so-called wave front method has been devised. The method was originally suggested by Rasmussen and Nielsen [14] for the case of a stationary force. The extensions to moving force problems will shortly be explained below. Normally, $\tilde{\mathbf{x}}$ is seen as a receiver point and $\tilde{\xi}$ as the source point. Alternatively, since the Green functions are only depending on the distance $r = |\tilde{\mathbf{x}} + \mathbf{v}(t-\tau) - \tilde{\xi}|$, we may consider $\tilde{\mathbf{x}}$ as the source point and $\tilde{\xi}$ as the receiver point, if only the sign of $\mathbf{v}$ is changed. Then, the result is that for a given position $\tilde{\mathbf{x}}$ at the time t, the integration is performed over a ring-shaped domain delimited by the P- and S-wave fronts emerging from the point $\tilde{\mathbf{x}}$. The idea is shown in Fig. 2 for the case of a stationary force ($\mathbf{v}=\mathbf{0}$), where the wave fronts are circles. Fig. 3 shows the variation of the field between the delimiting wave fronts. Because of the mentioned duality the hatched areas of Fig. 2 may also be considered as the source areas contributing to the receiver point $\tilde{\mathbf{x}}$ at various instants of time. Obviously, the numerical quadratures should concentrate on the hatched area where the integrand is non-zero. In the present case of a moving force the wave propagation is non-homogeneous, and the points $(\tilde{\xi}_1,\tilde{\xi}_2)$ on the wave fronts are placed on closed curves defined by the equation

$$\tilde{\xi}_2 = \tilde{x}_2 + v_2(t-\tau) \pm \sqrt{c^2(t-\tau)^2 - \left(\tilde{\xi}_1 - v_1(t-\tau) - \tilde{x}_1\right)^2}, \quad (14)$$

where $c = c_P$ or $c = c_S$.

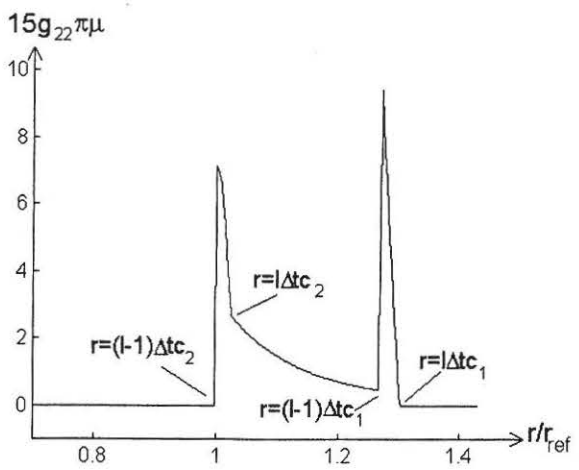

Fig. 3. Section of the wave front over which the integration is performed $r_{ref} = (l-1)\Delta t c_S$.

The integration is further enhanced by using directional subdivision, where each element is subdivided into a number of elements, and Gauss quadrature is used in each sub-element. The number of sub-elements, depends on the distance between the source point $\mathbf{x}$ and the element. The subdivision also depends on the order of the Gauss quadrature, which influences the magnitude of the error.

Evaluation of the singular integrals for the Green functions for $\tilde{\mathbf{x}} = \tilde{\xi}$ is performed using enclosing elements and the well-known rigid-body motion principle, see e.g. Ref. [1], using the fact that the singularities of the static Green's function and the elastodynamic Green's function for the traction are identical when approaching the singularities. The rigid-body motion principle will only work for interior problems with a closed boundary, due to the use of a rigid body motion. For problems with infinite boundaries the element mesh is extended with a fictitious enclosing boundary solely for the evaluation of the singular terms.

The BEM equations have been formulated for both the direct and indirect versions of the BEM in the time domain, see Ref. [14]. The direct BEM is the numerically solution of the Somigliana identity (13) after application of the boundary conditions. The indirect BEM also represents a discretization of the Somigliana identity but it formulates the problem in terms of some fictitious quantities denotes potentials.

4. Time approximation

For the time integration in Eq. (13) the time interval $[0,t]$ is divided into L subintervals, each of the length $\Delta t = t/L$. A linear variation of the field variables during each time step is assumed. Hereby two shape functions for the time integration are necessary and the following two integrals need to be evaluated analytically [13]

$$G_{ik}^{(1)} = \int_{t_{l-1}}^{t_l} g_{ik}(\tilde{\mathbf{x}} + \mathbf{v}(t-\tau), t-\tau; \tilde{\xi}, 0)(1-\kappa_l)\,\mathrm{d}\tau, \tag{15}$$

$$G_{ik}^{(2)} = \int_{t_{l-1}}^{t_l} g_{ik}(\tilde{\mathbf{x}} + \mathbf{v}(t-\tau), t-\tau; \tilde{\xi}, 0)\kappa_l\,\mathrm{d}\tau, \tag{16}$$

where the space integration has been omitted and $\kappa_l = (\tau - t_{l-1})/\Delta t$. Similar integrals appear for Green's function for the surface traction for a moving force.

Analytical integration of Eqs. (15) and (16), as well as the corresponding results involving the Green function for the surface traction is necessary since the later spatial integration into Eq. (13) will otherwise become unnecessarily complex, time consuming and inaccurate. The analytical integration of the discontinuous functions is made by splitting the integration up into several parts depending on the relationship between time variation of the discontinuous functions and the integration limits, see Ref. [13].

5. FEM solution with absorbing boundaries

A FEM formulation in convected coordinates is obtained by discretization of field differential equations similar to Eq. (6) for the displacement $\tilde{u}_i(\tilde{\mathbf{x}}_j, t)$. At the artificial boundaries of both the sides and the bottom of the mesh absorbing boundary conditions for the surface tension $\tilde{t}_i$ need to be specified as [7]

$$\tilde{t}_i = -Z_{ij}\left(\dot{\tilde{u}}_j - v_k \frac{\partial \tilde{u}_j}{\partial \tilde{x}_k}\right), \tag{17}$$

$$Z_{ij} = \frac{2\mu}{c_{\mathrm{P}}}\left(\tilde{n}_k r_k^{\mathrm{P}}\right) r_i^{\mathrm{P}} r_j^{\mathrm{P}} + \frac{\lambda}{c_{\mathrm{P}}}\tilde{n}_i r_j^{\mathrm{P}} + \frac{\mu}{c_{\mathrm{S}}}\left(\tilde{n}_k r_k^{\mathrm{S}}\right)\left(\delta_{ij} - 2 r_i^{\mathrm{S}} r_j^{\mathrm{S}}\right) + \frac{\mu}{c_{\mathrm{S}}} r_i^{\mathrm{S}} \tilde{n}_j. \tag{18}$$

The unit vector $r_i = r_i^{\mathrm{P}}$ or $r_i = r_i^{\mathrm{S}}$ signifies the direction of propagation in the fixed coordinate system of a P- or S-wave, which is initiated at the moving source at the time τ, and is hitting the boundary of the moving solution domain at the time t at a point with the moving coordinates $\tilde{x}_i$ and the outward directed unit vector $\tilde{n}_i$. $\tilde{x}_i$ signifies the direction of propagation as seen in the moving coordinate system. During the elapsed time interval $t-\tau$ the coordinate system and the wave have moved the distances $v_i\tau$ and $c\tau$, respectively, where $c = c_{\mathrm{P}}$ or $c = c_{\mathrm{S}}$. The vectors are related by the relation, see Fig. 1

$$c(t-\tau) r_i = v_i(t-\tau) + \tilde{x}_i \Rightarrow r_i = \frac{v_i}{c} + \frac{\tilde{x}_i}{c(t-\tau)}, \tag{19}$$

where

$$t - \tau = \frac{v_i \tilde{x}_i + \sqrt{(v_i \tilde{x}_i)^2 + |\tilde{\mathbf{x}}|\left(c^2 - |\mathbf{v}|^2\right)}}{c^2 - |\mathbf{v}|^2}. \tag{20}$$

The impedance boundary condition is asymptotically correct at large distances from the source and for high frequency impulses. However, it has proved effective even at distances and frequencies, where it was not expected to work. From its derivation the condition is not able to absorb Rayleigh-, Love- or Stoneley waves.

The final FEM equations are not symmetric due to the asymmetries from the convection terms in the field equations and due to the absorbing boundary conditions. This tend to destabilise the numerical results at large Mach-numbers ($M = \mathbf{v}/c_{\mathrm{S}}$) and has been cured

using a technique similar to the partial up-winding in Petrov–Galerkin variation, see Ref. [7].

Since the impedance boundary condition has been tuned to plane P- and S-waves. Therefore, Rayleigh, Love, Stoneley and non-plane P- and S-waves are partially reflected. The impedance boundary condition of the type (17) is not able to sustain static loading. Further, permanent displacements occur if the net impulse $\int_{-\infty}^{\infty} \mathbf{P}(t)\,dt \neq \mathbf{0}$, where $\mathbf{P}(t)$ is nodal loadings.

6. Numerical examples

In order to gauge the accuracy of the BEM scheme a convergence study of the BEM method has been performed for the case of the stationary force ($\mathbf{v} = \mathbf{0}$). The load consists of a distributed constant Heaviside type uniform line load acting in the positive x_1-direction on an isotropic, homogeneous, linear elastic 2D plane strain halfspace $x_2 > 0$. The distributed load per unit length $p(\tilde{\mathbf{x}}, t)$ is applied as

$$p(\tilde{\mathbf{x}}, t) = -p_0[H(\tilde{x}_1 + b) - H(\tilde{x}_1 - b)]H(t). \tag{21}$$

The analysis is performed using the following parameters: Intensity of line load $p_0 = 6.896 \times 10^4$ KN/m, $b = 76.2$ m, $\lambda = \mu = 6.895 \times 10^6$ KN/m^2 and $\rho = 3.151$ kg/m^3. This gives the wave velocities for the P- and S-waves, respectively, $c_P = 8.306 \times 10^2$ m/s and $c_S = 4.742 \times 10^2$ m/s, 762 m of the surface is discretized and the force is applied at the centre. The BEM mesh consists of 2 node, line elements with linear interpolation of width h, and h is varied through the values $h = 19$, 25, 38 and 76 m. A signifies the point $(\tilde{x}_1, \tilde{x}_2, \tilde{x}_3) = (0, 0, 0)$ at the center of the load, where the horizontal displacement $\tilde{u}_1 = 0$. The points B and C are placed 152 and 305 m to the right of the center of the load, respectively.

In Figs. 4 and 5 it is clear that no effects of reflections are present even for very large element sizes. Next the problem of a time-dependent load with zero net-impulse on an isotropic, homogenous linear elastic 2D plane strain halfspace is analysed using both the BEM and FEM approaches. The medium is subjected to a moving time dependent surface load per unit length $P(t)$. The time variation of the load is given as

$$P(t) = P_0\tau(1 - \tau^2)^2, \quad \tau = 2t/T - 1, \quad -1 < \tau < 1. \tag{22}$$

P_0 is the amplitude of the load, which appears almost sinusoidally with the period T. However, the load has vanishing derivatives at $t = 0$ and $t = T$. The example is performed with the following parameters: Intensity of force $P_0 = 1$ MN, $\mu = \lambda = 100 \times 10^6$ N/m^2 and $\rho = 2.0 \times 10^3$ kg/m^3. This gives the wave velocities for the P-, S- and Rayleigh waves, respectively, $c_P = 387$ m/s, $c_S = 224$ m/s and $c_R = 206$ m/s, 60 m of the surface are discretized and the force is applied at the centre. The applied FEM mesh is rectangular with a depth of 80 m. The BEM mesh consists of 4 m, 2 node, line elements with linear interpolation and similarly the FEM mesh consists of 4 m × 4 m, 4 node quadrilateral elements, see Fig. 6a and b.

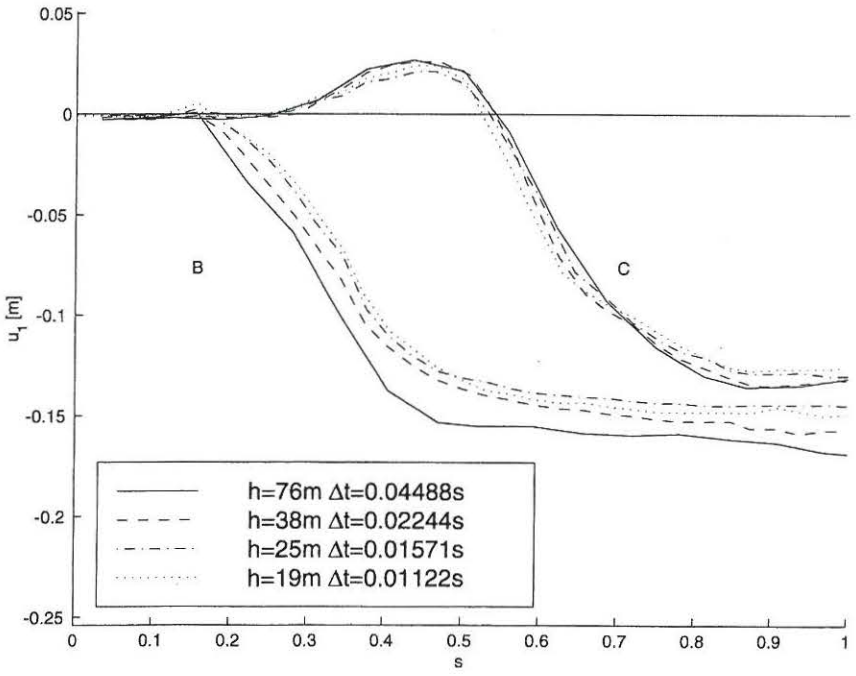

Fig. 4. Horizontal displacements at B: $(\tilde{x}_1, \tilde{x}_2, \tilde{x}_3) = (152\text{ m}, 0\text{ m}, 0\text{ m})$, C: $(\tilde{x}_1, \tilde{x}_2, \tilde{x}_3) = (305\text{ m}, 0\text{ m}, 0\text{ m})$.

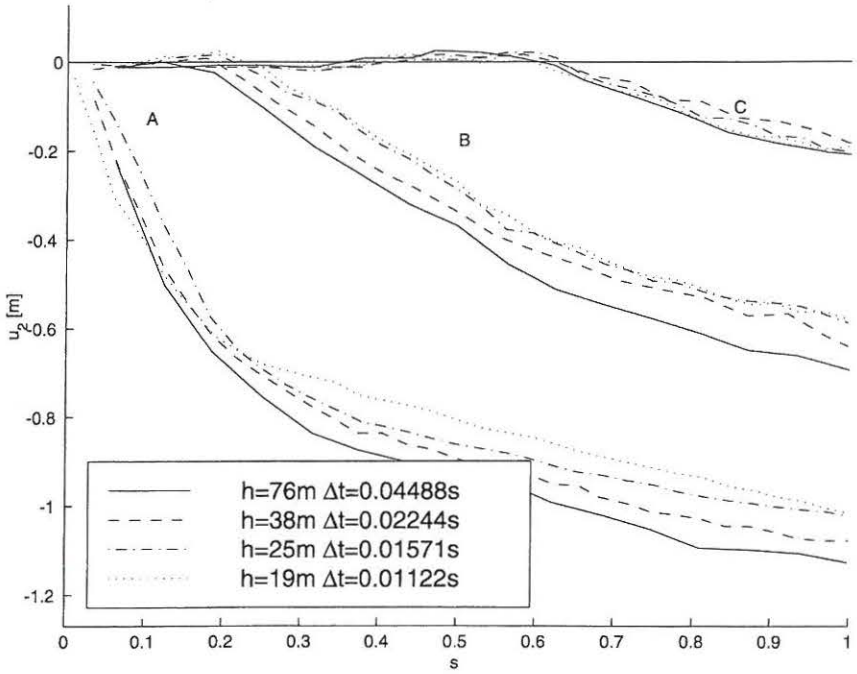

Fig. 5. Vertical displacements at A: $(\tilde{x}_1, \tilde{x}_2, \tilde{x}_3) = (0\text{ m}, 0\text{ m}, 0\text{ m})$; B: $(\tilde{x}_1, \tilde{x}_2, \tilde{x}_3) = (152\text{ m}, 0\text{ m}, 0\text{ m})$; C: $(\tilde{x}_1, \tilde{x}_2, \tilde{x}_3) = (305\text{ m}, 0\text{ m}, 0\text{ m})$.

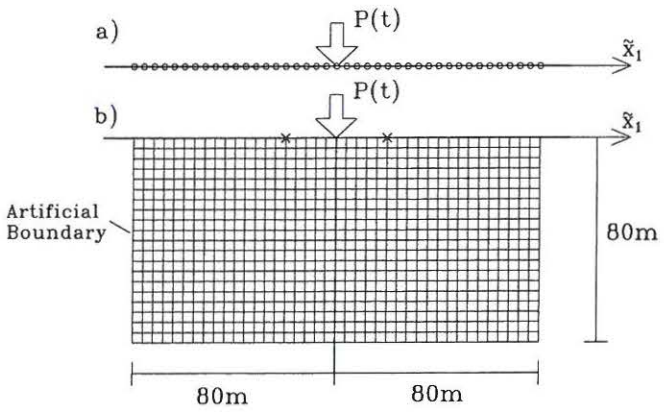

Fig. 6. (a) BEM and (b) FEM meshes.

The horizontal, $\tilde{u}_1$ and vertical, $\tilde{u}_2$ displacement histories at $(\tilde{x}_1, \tilde{x}_2, \tilde{x}_3) = (+20\text{ m}, 0\text{ m}, 0\text{ m})$, 'in front of the force' and at $(\tilde{x}_1, \tilde{x}_2, \tilde{x}_3) = (-20\text{ m}, 0\text{ m}, 0\text{ m})$, 'behind the force' are presented in the following figures. The applied counter measure to stabilize the FEM scheme due to the convection terms is tantamount to the introduction of artificial numerical damping, which may change the magnitude of the observed response slightly. This defect should be kept in mind in the following comparison with the BEM solution. Comparison between Figs. 7 and 8 shows that both the minimum and maximum displacements decrease with greater speed. However, for $v_1 = 0c_S$ in Fig. 7, the BEM results for the minimum displacements are significantly smaller than the equivalent minima from the FEM results.

In all the Figs. 7–10, but especially in Fig. 10, the FEM results show tendencies to reflect Rayleigh waves from the boundaries. However, the BEM results do not show any signs of reflection in any of the figures. The calculation time for the FEM solution was 62 s on a 200 MHz PC while the calculation time for the BEM solution was several hours on a SiliconGraphics Indy R4400. In Figs. 11 and 12 the FEM and BEM results for velocities approaching the Rayleigh wave velocity are shown 'in front of the force'.

The Rayleigh wave velocity for Poisson materials ($\mu = \lambda$) is approximately $0.92c_S$. The results for velocities approaching the Rayleigh wave velocity are shown for a point only 4 m in front of force. The reason for this change is that the wavefront in front of the force at the surface do not move very far from the force when the force moves almost as fast as the Rayleigh wave. Krylov [8] assumes that the displacements increases dramatically when the velocity approach the Rayleigh wave velocity. The results in Figs. 11 and 12 obviously disagrees with that statement. Actually, the displacements decreases compared to the results obtained with lower velocities shown in Figs. 7–10.

7. Conclusion

A new BEM formulation in a moving coordinate system has been given. The formulation introduces Green's functions for a moving force and shows how the

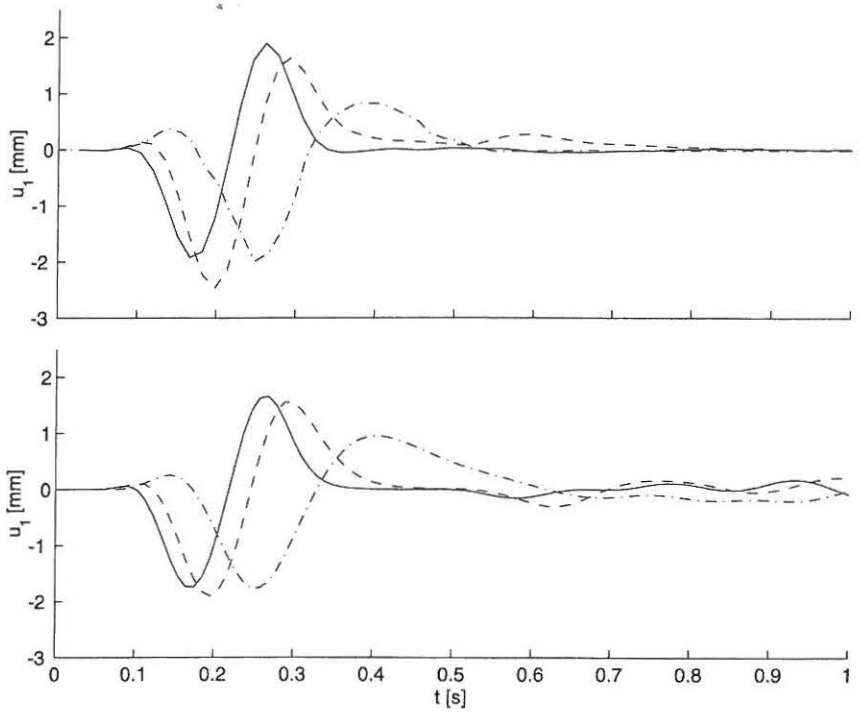

Fig. 7. Horizontal displacements at $(\tilde{x}_1, \tilde{x}_2, \tilde{x}_3) = (+20\text{ m}, 0\text{ m}, 0\text{ m})$ obtained using BEM (top) and FEM (bottom) for $v_1 = 0$ (—), $v_1 = 0.2c_S$ (– – –) and $v_1 = 0.5c_S$ (– · – · –).

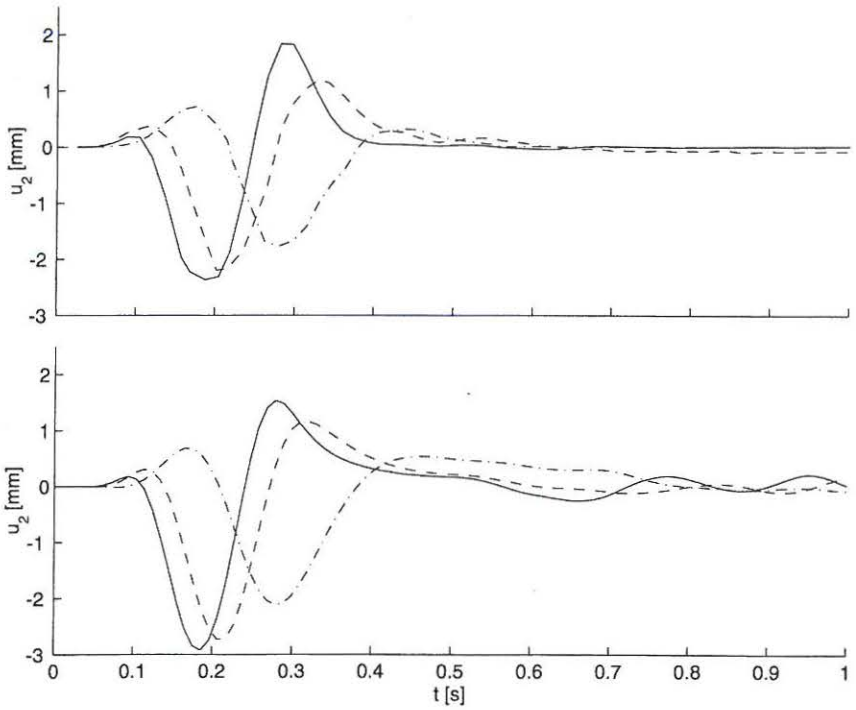

Fig. 8. Vertical displacements at $(\tilde{x}_1, \tilde{x}_2, \tilde{x}_3) = (+20\text{ m}, 0\text{ m}, 0\text{ m})$ obtained using BEM (top) and FEM (bottom) for $v_1 = 0$ (—), $v_1 = 0.2c_S$ (– – –) and $v_1 = 0.5c_S$ (– · – · –).

normal BEM formulation for a fixed coordinate system can be modified to a formulation in the moving coordinate system by using the Green functions for a moving force.

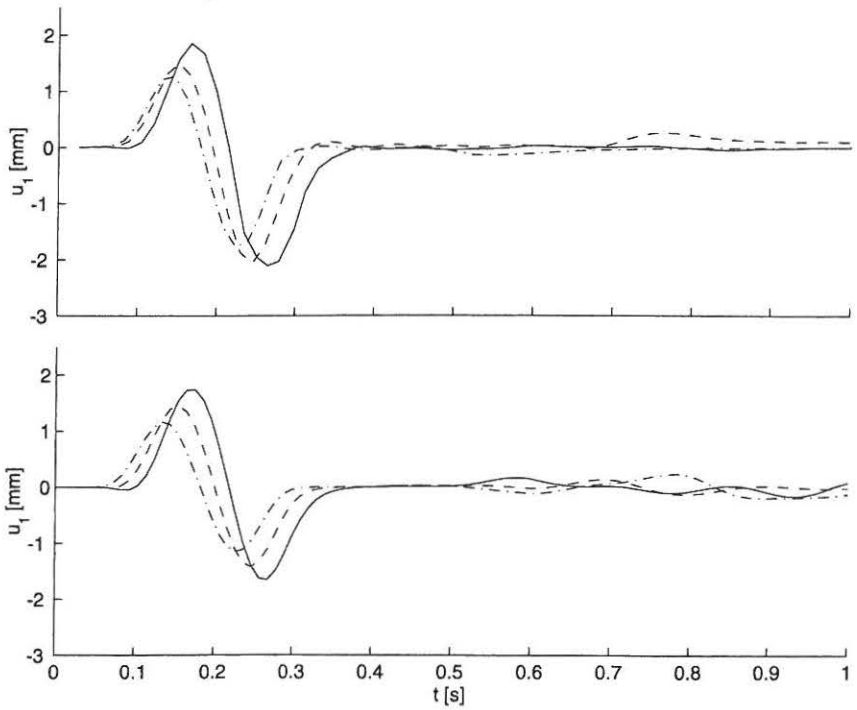

Fig. 9. Horizontal displacements at $(\tilde{x}_1, \tilde{x}_2, \tilde{x}_3) = (-20\text{ m}, 0\text{ m}, 0\text{ m})$ obtained using BEM (top) and FEM (bottom) for $v_l = 0$ (—), $v_l = 0.2c_S$ (– – –) and $v_l = 0.5c_S$ (– · – · –).

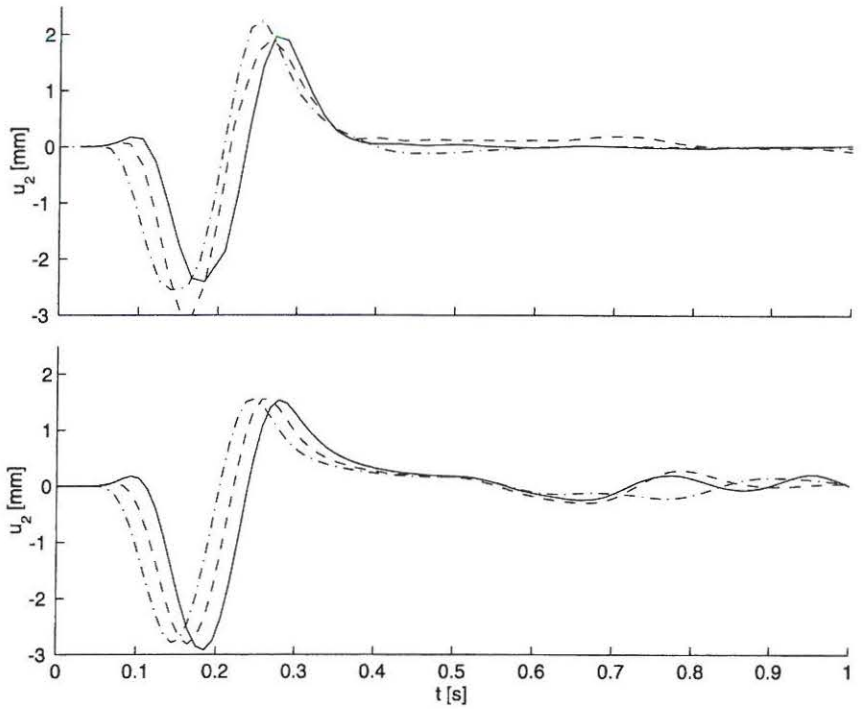

Fig. 10. Vertical displacements at $(\tilde{x}_1, \tilde{x}_2, \tilde{x}_3) = (-20\text{ m}, 0\text{ m}, 0\text{ m})$ obtained using BEM (top) and FEM (bottom) for $v_l = 0$ (—), $v_l = 0.2c_S$ (– – –) and $v_l = 0.5c_S$ (– · – · –).

The BEM results have been compared to results obtained by a FEM formulation using an impedance boundary condition as absorbing boundary. The results from the BEM and FEM formulation show good agreement for a simple stress wave propagation problem with a moving force and it is demonstrated that the

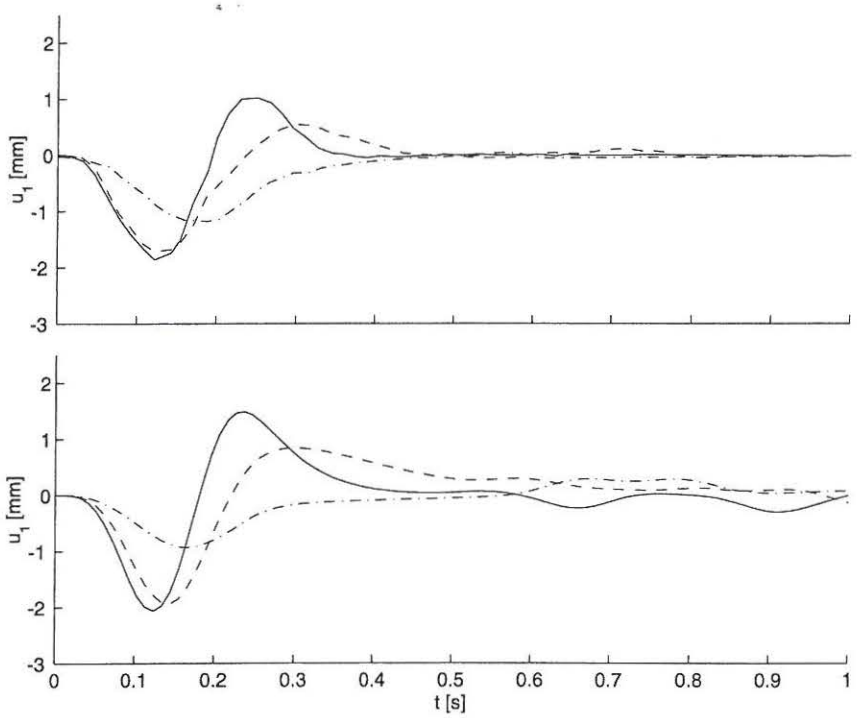

Fig. 11. Horizontal displacements at $(\tilde{x}_1, \tilde{x}_2, \tilde{x}_3) = (+4\text{ m}, 0\text{ m}, 0\text{ m})$ obtained using BEM (top) and FEM (bottom) for $v_l = 0.5c_S$ (—), $v_l = 0.7c_S$ (– – –) and $v_l = 0.9c_S$ (– · – · –).

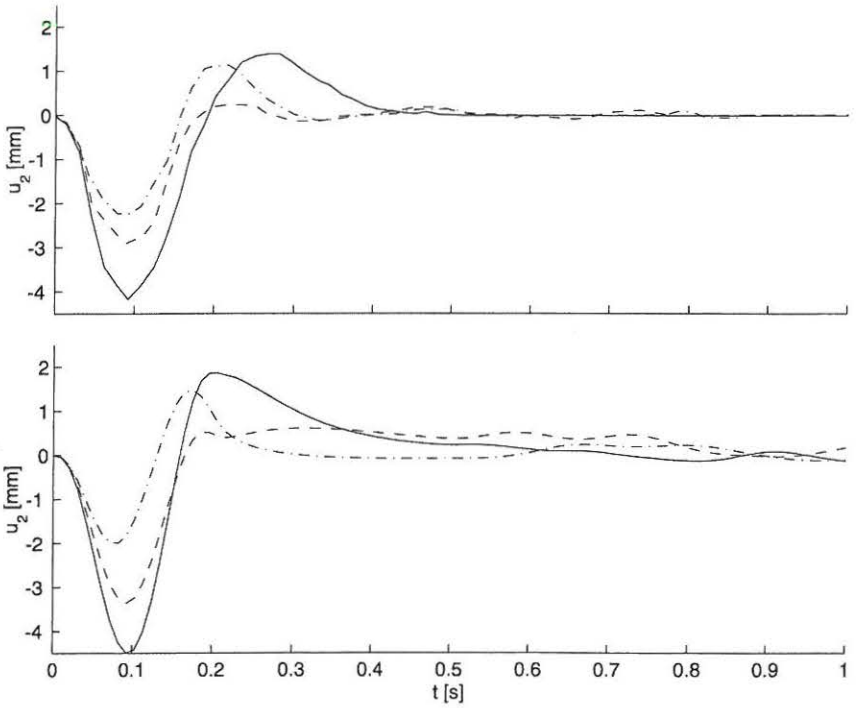

Fig. 12. Vertical displacements at $(\tilde{x}_1, \tilde{x}_2, \tilde{x}_3) = (+4\text{ m}, 0\text{ m}, 0\text{ m})$ obtained using BEM (top) and FEM (bottom) for $v_l = 0.5c_S$ (—), $v_l = 0.7c_S$ (– – –) and $v_l = 0.9c_S$ (– · – · –).

reflection of Rayleigh waves is omitted in the BEM analysis. Another finding is that the displacements do not increase when the velocity approaches the Rayleigh wave velocity as is often postulated.

Acknowledgements

The present research was partially supported by The Danish Technical Research Council within the project: Damping Mechanisms in Dynamics of Structures and Materials.

References

[1] Banerjee PK, Ahmad S, Manolis GD. Advanced elastodynamic analysis. Computational methods in mechanics, vol II. In: Beskos DE. editor. Boundary Element Methods in Mechanics. Amsterdam: Elsevier; 1987.

[2] Beskos DE, Vardoulakis IG. Vibration isolation of structures from surface waves. In: Yagawa G. editor. Computational Mechanics 86. Berlin: Springer; 1986.

[3] Beskos DE. Boundary element methods in dynamic analysis: Part II 1986–1996. Appl Mech Reviews 1997; 50:149–97.

[4] Chouw N, Le R, Schmid G. Reduction of train-induced vibrations and waves. Germany: Ruhr-University Bochum; 1993.

[5] Eringen AC, Suhubi ES. Elastodynamics. vol II, Linear Theory. New York: Academic Press; 1975.

[6] Fryba L. Vibration of solids and structures under moving loads. Acedemia Pragh, 1999.

[7] Krenk S, Kellezi L, Nielsen SRK, Kirkegaard PH. Finite element and transmitting boundary conditions for moving loads. Proceedings of the Fourth European Conference on Structural Dynamics, Eurodyn'99, Praha, 1999. p. 447–52.

[8] Krylov V. Generation of ground vibrations by superfast trains. Appl Acoustics 1995;44:149–64.

[9] Madshus C, Bessason B, Hårvik L. Prediction model for low frequency vibration from high speed railways on soft ground. J Sound Vibr 1996;193(1):195–203.

[10] Nelson JT. Recent developments in ground-borne noise and vibration control. J Sound Vibr 1996;193(1):367–76.

[11] Okumura Y, Kuno K. Statistical analysis of field data of railway noise and vibration collected in an urban area. Appl Acoustics 1991;33:263–80.

[12] Pan G, Atluri SN. Dynamic response of finite sized elastic runways subjected to moving loads: a coupled BEM/FEM approach. Int J Numer Methods Engng 1995;38:3143–66.

[13] Rasmussen KM. Stress wave propagation in soils modelled by the boundary element method. PhD Thesis, Aalborg University, 1999.

[14] Rasmussen KM, Nielsen SRK. 2D time domain boundary element direct and indirect formulation applied to soil dynamics. Proceedings of the 13th International Conference on Boundary Element Technology, BETECH 99, Las Vegas, 1999. p. 195–204.

[15] Suiker ASJ, Chang SC, de Borst R, Esveld C. Surface waves in a stratified half space with enchanced continuum properties Part 1: formulation of the boundary value problem. Euro J Mech Solids 1999;18:749–68.

[16] Suiker ASJ, Chang SC, de Borst R, Esveld C. Surface waves in a stratified half space with enchanced continuum properties Part 2: analysis of the wave characteristics in regard to high-speed railway tracks. Euro J Mech Solids 1999;18:769–84.

[17] Trochides A. Ground-borne vibrations in buildings near subways. Appl Acoustics 1991;32:289–96.